

Discontinuous Galerkin methods for a dispersive wave hydro-sediment-morphodynamic model

Kazbek Kazhyken^{a,*}, Juha Videman^b, Clint Dawson^a

^a*Oden Institute for Computational Engineering and Sciences, The University of Texas at Austin, Austin, TX 78712, USA*

^b*CAMGSD/Departamento de Matemática, Universidade de Lisboa, Universidade de Lisboa, 1049-001 Lisbon, Portugal*

Abstract

A dispersive wave hydro-sediment-morphodynamic model developed by complementing the shallow water hydro-sediment-morphodynamic (SHSM) equations with the dispersive term from the Green-Naghdi equations is presented. A numerical solution algorithm for the model based on the second-order Strang operator splitting is presented. The model is partitioned into two parts, (1) the SHSM equations and (2) the dispersive correction part, which are discretized using discontinuous Galerkin finite element methods. This splitting technique provides a facility to select dynamically regions of a problem domain where the dispersive term is not applied, e.g. wave breaking regions where the dispersive wave model is no longer valid. Algorithms that can handle wetting-drying and detect wave breaking are provided and a number of numerical examples are presented to validate the developed numerical solution algorithm. The results of the simulations indicate that the model is capable of predicting sediment transport and bed morphodynamic processes correctly provided that the empirical models for the suspended and bed load transport are properly calibrated. Moreover, the developed model is able to accurately capture hydrodynamics and wave dispersion effects up to swash zones, and its application is justified for simulations where dispersive wave effects are prevalent.

Keywords: Green-Naghdi equations, SHSM equations, dispersive waves, sediment transport, discontinuous Galerkin methods

1. Introduction

A sediment transport process in coastal applications is a type of a two-phase fluid-solid flow with sea water as the fluid and pebbles and stones of varying sizes, and quartz sand as the solid. There are three modes of sediment transport: bed load, suspended load, and wash load transport. The bed load transport

*Corresponding author

Email address: kazbek@oden.utexas.edu (Kazbek Kazhyken)

is characterized by motion of the sediment particles without detaching from the sediment bed for a significant amount of time, i.e. the sediment particles move by sliding, rolling, and saltating. There are a number of empirical models developed for the bed load transport, for example Meyer-Peter and Mueller [1], Fernandez Luque and Van Beek [2], Nielsen [3], Ribberink [4]. In the suspended load transport, the sediment particles suspended in water are advected with the water flow. These sediment particles, which are typically of a fine silt and clay size, remain suspended in water by turbulent flows and require a significant amount of time to settle on the sediment bed. Sediment particles in the wash load are transported without deposition while remaining close to the water surface in near-permanent suspension. Due to a limited effect of the wash load on the sediment bed morphology, effects of the wash load transport are not considered in the presented work.

Hydrodynamic, sediment transport, and bed morphodynamic processes are closely interrelated: hydrodynamic parameters of a water flow affect sediment transport rates, these rates influence the bed morphology that in its turn affects the water flow and sediment transport. These hydro-sediment-morphodynamic processes driven by astronomical tides, winds, and long-wave currents in coastal areas attract a high degree of interest since morphological changes of a coastal area can negatively affect its infrastructure and environment. Elements of coastal infrastructure, such as bridges, piers, and levees, can become structurally compromised as a result of excessive erosion of the sediment bed due to scouring. Environmental concerns include shoreline and beach erosion that may damage natural habitats of endangered protected species, and the effect of sediment transport on contaminants, i.e. sediment deposits may serve as dangerous contaminant sinks or sources. It is thus evident that mathematical modeling of hydro-sediment-morphodynamic processes in coastal areas has clear engineering relevance. Deriving such models poses, however, a number of challenges since they have to couple non-linear hydrodynamic, sediment transport, and bed morphodynamic equations along with modeling their two-way interactions.

A number of hydro-sediment-morphodynamic models, ranging from one to three dimensional models, have been developed for coastal applications over the last four decades. These models are discussed in detail in [5] and [6]. A three-dimensional model has the capacity for a more accurate and detailed resolution of the process [7, 8, 9]; however, the amount of computational resources required to run any sizable simulation with such a model is prohibitively large. Therefore, application of three-dimensional models is typically limited to short-time simulations over small-size domains. As an alternative, a depth averaged two- or, in some cases, one-dimensional model can be used to resolve hydro-sediment-morphodynamic processes in coastal areas. One such model is formed by the shallow water hydro-sediment-morphodynamic (SHSM) equations, which are derived by integrating and averaging the three-dimensional mass and momentum conservation equations of motion (e.g. see Wu [10]). In the SHSM equations, the nonlinear shallow water equations, which resolve water-sediment mixture hydrodynamics, are fully coupled with sediment transport and bed morphodynamic models (see Cao *et al.* [11] for variations of the SHSM equations).

Within the last decade, the SHSM equations have been successfully applied in studies of coastal hydro-sediment-morphodynamic processes (e.g. Xiao *et al.*, 2010 [12], Zhu and Dodd, 2015 [13], Kim, 2015 [14], Incelli *et al.*, 2016 [15], Briganti *et al.*, 2016 [16]).

Numerical solution algorithms for the SHSM equations are typically developed with finite volume methods for applications with unstructured grids. Cao *et al.* [17] use the total-variation-diminishing (TVD) weighted average flux method (WAF) in conjunction with the Harten-Lax-van Leer-contact (HLLC) approximate Riemann solver to develop their numerical solution algorithm for the SHSM equations. Examples of works that employ HLLC as an approximate Riemann solver for numerical flux definitions include [18], [19], and [20]. Algorithms based on upwinding numerical fluxes and Roe-averaged states are developed in [21] and [22]. Liu *et al.* [23], [24], [25] develop numerical methods for the SHSM equations that employ a central-upwind scheme along with the Lagrange theorem to approximate the upper and lower bounds of the local wave speeds. Xia *et al.* [26] use the operator-splitting technique for the source term and the FORCE (first-order centered) approximate Riemann solver for a numerical treatment of the model. Discontinuous Galerkin discretizations of the SHSM equations are used less often, see, *e.g.*, [27] and [28].

The nonlinear shallow water equations, which form the hydrodynamic part of the SHSM equations, have a number of advantages: a capacity to approximate water motion with a sufficient accuracy in the shallow water flow regime, a plethora of developed numerical solution algorithms (e.g. Zhao *et al.* [29], Anastasiou and Chan [30], Sleigh *et al.*, [31], Aizinger and Dawson [32], Yoon and Kang [33], Kubatko *et al.* [34], Samii *et al.* [35]), efficient parallelization strategies (e.g. hybrid MPI+OpenMP and HPX parallelization in Bremer *et al.* [36]), and its ability to approximate wave breaking effects in surf zones. However, this hydrodynamic model does not have a capacity to capture wave dispersion effects; and, therefore, an application of the SHSM equations is not feasible in areas where the dispersion effects are prevalent. An alternative depth-averaged hydrodynamic model that can reproduce dispersion effects is formed by the Green-Naghdi equations developed in [37]. A number of numerical solution algorithms exist for the Green-Naghdi equations that use various discretization techniques, from finite difference to finite element methods, and a Strang operator splitting technique (e.g. see [38, 39, 40, 41, 42, 43, 44, 45]). The use of a Strang operator splitting in these algorithms provides the capacity to switch between the nonlinear shallow water equations and the Green-Naghdi equations whenever one of the hydrodynamic models is more accurate than the other [42].

The purpose of the presented work is to introduce dispersive wave effects into the SHSM equations. This is achieved through considering the Green-Naghdi equations which results in a dispersive wave hydro-sediment-morphodynamic model. Since the difference between the nonlinear shallow water equations and the Green-Naghdi equations is constituted by the dispersive term defined through a differential operator that forms an elliptic system [39], this new model is formed by incorporating the dispersive term into the SHSM equations. The resulting model has the potential to be used in the simulation of morphody-

dynamic processes in areas where dispersive wave effects are prevalent. Numerical solution algorithms for this model are developed employing a Strang operator splitting technique and discontinuous Galerkin finite element methods. A significant portion of this work comprises the development of a massively parallel solver that uses the developed numerical solution algorithms. The solver extends a C++ software package developed by Bremer and Kazhyken¹.

The rest of the paper is organized as follows. Section 2 presents the governing equations for the dispersive wave hydro-sediment-morphodynamic model. The developed numerical solution algorithms are introduced in Section 3. Section 4 presents a number of numerical tests, including one-dimensional and two-dimensional dam break simulations and solitary wave runs over an erodible sloping beach, that are used to perform verification and validation of the developed algorithms. Final conclusions are presented in Section 5.

2. Governing equations

A body of water can be represented by a domain $D_t \subset \mathbb{R}^{d+1}$, where d is the horizontal spatial dimension that can take values 1 or 2, and t represents the time variable. The domain D_t is filled with a water-sediment mixture, modeled as an incompressible inviscid fluid, and bounded vertically by the bottom and top boundaries, Γ_B and Γ_T , which the fluid particles cannot cross (cf. Fig.1). It is assumed that Γ_B and Γ_T can be represented as graphs that vary in time: Γ_B due to sediment transport and bed morphodynamic processes, Γ_T as the evolving free surface of the body of water. The bathymetry, $b(X, t)$, and the free surface elevation, $\zeta(X, t)$, of the body of water are used in the parameterization of Γ_B and Γ_T :

$$\Gamma_B = \{(X, -H_0 + b(X, t)) : X \in \mathbb{R}^d\}, \quad (1a)$$

$$\Gamma_T = \{(X, \zeta(X, t)) : X \in \mathbb{R}^d\}, \quad (1b)$$

and the domain D_t is defined as a set of points $(X, z) \in \mathbb{R}^d \times \mathbb{R}$ where $-H_0 + b(X, t) < z < \zeta(X, t)$.

A depth-averaged model that can resolve water wave dynamics, and subsequent sediment transport and bed evolution in the domain D_t is the shallow water hydro-sediment-morphodynamic (SHSM) equations (e.g. see Cao *et al.* [17]). The hydrodynamic part of the equations is represented by the nonlinear shallow water equations, which provide a sufficiently accurate approximation to the water wave dynamics whenever the shallowness parameter $\mu = H_0^2/L_0^2$, where L_0 is the characteristic length, and H_0 is the reference depth, is less than unity. The present work aims to develop a hydro-sediment-morphodynamic model that has the capacity to capture wave dispersion effects, which the nonlinear shallow water equations are unable to resolve. Therefore, the nonlinear

¹The software is under development on the date of the publication, and can be accessed at www.github.com/UT-CHG/dgswemv2. Should there be any questions, comments, or suggestions, please contact the developers through the repository issues page.

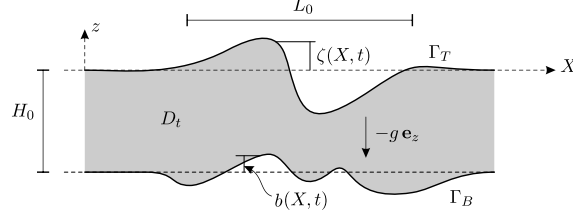


Figure 1: A model representation of a body of water as a domain $D_t \subset \mathbb{R}^{d+1}$.

shallow water equations in the SHSM model are replaced with a single parameter variation of the Green-Naghdi equations, a depth-averaged hydrodynamic model which has the capacity to capture wave dispersion effects, introduced by Bonneton *et al.* in [39]. This forms a set of equations defined over a horizontal domain $\Omega \subset \mathbb{R}^d$:

$$\partial_t \mathbf{q} + \nabla \cdot \mathbf{F}(\mathbf{q}) + \mathbf{D}(\mathbf{q}) = \mathbf{S}(\mathbf{q}), \quad (2)$$

where the vector of unknowns \mathbf{q} and the flux matrix $\mathbf{F}(\mathbf{q})$ are

$$\mathbf{q} = \begin{Bmatrix} h \\ h\mathbf{u} \\ hc \\ b \end{Bmatrix}, \quad \mathbf{F}(\mathbf{q}) = \begin{Bmatrix} h\mathbf{u} \\ h\mathbf{u} \otimes \mathbf{u} + \frac{1}{2}gh^2\mathbf{I} \\ hc\mathbf{u} \\ \mathbf{q}_b \end{Bmatrix}, \quad (3)$$

the source term $\mathbf{S}(\mathbf{q})$ is defined as

$$\mathbf{S}(\mathbf{q}) = \begin{Bmatrix} -gh\nabla b - \frac{\rho_s - \rho_w}{2\rho} gh^2 \nabla c - \frac{(\rho_0 - \rho)(E - D)}{\rho(1-p)} \mathbf{u} + \mathbf{f} \\ E - D \\ -\frac{E - D}{1-p} \end{Bmatrix}, \quad (4)$$

\mathbf{u} is the water velocity represented by a d dimensional vector and h is the water depth represented by the mapping $h(X, t) = \zeta(X, t) + H_0 - b(X, t)$ and assumed to be bounded from below by a positive value. Moreover, c is the volume concentration of sediment in water-sediment mixture, E and D are the sediment entrainment and deposition rates, respectively, p is the bed porosity, ρ_w and ρ_s are the water and the sediment densities, ρ and ρ_0 are the water-sediment mixture and saturated bed densities defined as $\rho = (1 - c)\rho_w + c\rho_s$ and $\rho_0 = (1 - p)\rho_s + p\rho_w$, \mathbf{q}_b is the bed load sediment flux, \mathbf{f} comprises additional source terms for the momentum continuity equation (e.g. the Coriolis, bottom friction, and surface wind stress forces), g is the acceleration due to gravity, and $\mathbf{I} \in \mathbb{R}^{d \times d}$ is the identity matrix. Finally, the wave dispersion effects are

introduced into the model through the dispersive term

$$\mathbf{D}(\mathbf{q}) = \begin{Bmatrix} 0 \\ \mathbf{w}_1 - \alpha^{-1}gh\nabla\zeta \\ 0 \\ 0 \end{Bmatrix}, \quad (5)$$

where \mathbf{w}_1 is defined through an elliptic system

$$(\mathbf{I} + \alpha h \mathcal{T} h^{-1}) \mathbf{w}_1 = \alpha^{-1}gh\nabla\zeta + h\mathcal{Q}_1(\mathbf{u}), \quad (6)$$

with operators \mathcal{T} and \mathcal{Q}_1 defined as

$$\mathcal{T}(\mathbf{w}) = \mathcal{R}_1(\nabla \cdot \mathbf{w}) + \mathcal{R}_2(\nabla b \cdot \mathbf{w}), \quad (7a)$$

$$\mathcal{Q}_1(\mathbf{w}) = -2\mathcal{R}_1(\partial_x \mathbf{w} \cdot \partial_y \mathbf{w}^\perp + (\nabla \cdot \mathbf{w})^2) + \mathcal{R}_2(\mathbf{w} \cdot (\mathbf{w} \cdot \nabla) \nabla b), \quad (7b)$$

where operators \mathcal{R}_1 and \mathcal{R}_2 are

$$\mathcal{R}_1(w) = -\frac{1}{3h}\nabla(h^3w) - \frac{h}{2}w\nabla b, \quad (8a)$$

$$\mathcal{R}_2(w) = \frac{1}{2h}\nabla(h^2w) + w\nabla b, \quad (8b)$$

and $\mathbf{w}^\perp = (-w_2, w_1)^\mathbf{T}$. Parameter $\alpha \in \mathbb{R}$ in the dispersive term is used to optimize dispersive properties of the presented hydro-sediment-morphodynamic model. By adjusting α , the difference between the phase and group velocities coming from the Stokes linear theory and the Green-Naghdi equations can be minimized. A common strategy aims at minimizing the averaged variation over some range of wave number values [39].

In the presented model E , D and \mathbf{q}_b are defined through empirical equations. The sediment entrainment rate E may be defined as in [46]:

$$E = \begin{cases} \phi(\theta - \theta_c)|\mathbf{u}|h & \text{if } \theta > \theta_c \\ 0 & \text{if } \theta \leq \theta_c \end{cases}, \quad (9)$$

where ϕ is a calibration parameter, θ_c is the critical Shields parameter and θ is the Shields parameter given by $\theta = |\boldsymbol{\tau}_b|/\sqrt{sgd_{50}}$, where $\boldsymbol{\tau}_b$ is the bottom friction, $s = \rho_s/\rho_w - 1$ is the submerged specific gravity, and d_{50} is the mean sediment particle size. The sediment deposition rate D can be estimated by an empirical model from [17]:

$$D = \omega_o C_a (1 - C_a)^2, \quad (10)$$

where ω_o is the setting velocity of a sediment particle in still water, and $C_a = \alpha\alpha_c$ is the near-bed sediment volume concentration with the coefficient $\alpha_c = \min(2, (1-p)/c)$. A number of empirical models for \mathbf{q}_b is proposed as (see [47, 48] and all the references therein)

$$\mathbf{q}_b = A(h, \mathbf{u})|\mathbf{u}|^{m-1}, \quad (11)$$

where $1 \leq m \leq 3$ and $A(h, \mathbf{u})$ is an empirical equation, e.g. the Grass model takes A as a constant calibrated for the application under investigation and sets $m = 3$, cf. [49].

3. Numerical methods

Discontinuous Galerkin finite element methods are used to discretize the governing equations. This choice facilitates the use of unstructured meshes that are well suited for irregular geometries of coastal areas. Thus, the problem domain Ω is partitioned into a finite element mesh $\mathcal{T}_h = \{K\}$ that provides an approximation to the domain:

$$\Omega \approx \Omega_h = \sum_{K \in \mathcal{T}_h} K, \quad (12)$$

where the subscript h stands for the mesh parameter represented by the diameter of the smallest element in the mesh. The set of all mesh element faces, $\partial\mathcal{T}_h$, and the set of all edges of the mesh skeleton, \mathcal{E}_h , are defined as

$$\partial\mathcal{T}_h = \{\partial K : K \in \mathcal{T}_h\}, \quad (13a)$$

$$\mathcal{E}_h = \{e \in \bigcup_{K \in \mathcal{T}_h} \partial K\}. \quad (13b)$$

Note that in \mathcal{E}_h the common element faces appear only once but in $\partial\mathcal{T}_h$ they are counted twice.

To develop variational formulations of the governing equations, inner products are defined for finite dimensional vectors \mathbf{u} and \mathbf{v} through:

$$(\mathbf{u}, \mathbf{v})_\Omega = \int_\Omega \mathbf{u} \cdot \mathbf{v} \, dX, \quad (14a)$$

$$\langle \mathbf{u}, \mathbf{v} \rangle_{\partial\Omega} = \int_{\partial\Omega} \mathbf{u} \cdot \mathbf{v} \, dX, \quad (14b)$$

for $\Omega \subset \mathbb{R}^d$ and $\partial\Omega \subset \mathbb{R}^{d-1}$.

An approximating space of trial and test functions is chosen as the set of square integrable functions over Ω_h such that their restriction to an element K belongs to $\mathcal{Q}^p(K)$, a space of polynomials of degree at most $p \geq 0$ with support in K :

$$\mathbf{V}_h^{p,m} := \{\mathbf{v} \in (L^2(\Omega_h))^m : \mathbf{v}|_K \in (\mathcal{Q}^p(K))^m \quad \forall K \in \mathcal{T}_h\}, \quad (15)$$

and, similarly, an approximation space over the mesh skeleton is chosen as

$$\mathbf{M}_h^{p,m} := \{\boldsymbol{\mu} \in (L^2(\mathcal{E}_h))^m : \boldsymbol{\mu}|_e \in (\mathcal{Q}^p(e))^m \quad \forall e \in \mathcal{E}_h\}. \quad (16)$$

A Strang operator splitting technique is used in the numerical solution of the hydro-sediment-morphodynamic model presented in Eq.(2). To this end, the model is split into two separate parts: (1) the SHSM equations obtained by dropping the dispersive term of the equations, and (2) the dispersive correction part where the wave dispersion effects on flow velocities are introduced into the model through the dispersive term. If \mathcal{S}_1 is a numerical solution operator for the SHSM equations, i.e. $\mathcal{S}_1(\Delta t)$ propagates numerical solution by a time step Δt , and, similarly, \mathcal{S}_2 is a numerical solution operator for the dispersive

correction part, then the numerical solution operator for the full hydro-sediment-morphodynamic model in Eq.(2) can be approximated with the Strang operator splitting technique [50]:

$$\mathcal{S}(\Delta t) = \mathcal{S}_1(\Delta t/2)\mathcal{S}_2(\Delta t)\mathcal{S}_1(\Delta t/2), \quad (17)$$

where \mathcal{S} is a second-order temporal discretization if both \mathcal{S}_1 and \mathcal{S}_2 use a second-order time discretization method.

A numerical solution operator \mathcal{S}_1 for the SHSM equations is developed using a discontinuous Galerkin finite element formulation where an approximate solution $\mathbf{q}_h \in \mathbf{V}_h^{p,d+3}$ is sought such that it satisfies the variational formulation

$$(\partial_t \mathbf{q}_h, \mathbf{v})_{\mathcal{T}_h} - (\mathbf{F}_h, \nabla \mathbf{v})_{\mathcal{T}_h} + \langle \mathbf{F}_h^*, \mathbf{v} \rangle_{\partial \mathcal{T}_h} - (\mathbf{S}_h, \mathbf{v})_{\mathcal{T}_h} = 0 \quad \forall \mathbf{v} \in \mathbf{V}_h^{p,d+3}, \quad (18)$$

where $\mathbf{F}_h = \mathbf{F}(\mathbf{q}_h)$ and $\mathbf{S}_h = \mathbf{S}(\mathbf{q}_h)$, \mathbf{F}_h^* is a single valued approximation to $\mathbf{F}_h \mathbf{n}$ over element faces, called the numerical flux, and \mathbf{n} is the unit outward normal vector to element face. To define the numerical flux, the bed update part of the SHSM equations is singled out for a separate treatment. The numerical flux for this formulation is then defined as

$$\mathbf{F}_h^* = \left\{ \begin{matrix} \mathbf{G}_h^* \\ \mathbf{q}_b^* \end{matrix} \right\}, \quad (19)$$

where \mathbf{q}_b^* is the numerical bed load flux, and \mathbf{G}_h^* is the numerical flux for the remaining part of the system where the vector of unknowns \mathbf{r} and the flux matrix $\mathbf{G}(\mathbf{r})$ are

$$\mathbf{r} = \left\{ \begin{matrix} h \\ h\mathbf{u} \\ hc \end{matrix} \right\}, \quad \mathbf{G}(\mathbf{r}) = \left\{ \begin{matrix} h\mathbf{u} \\ h\mathbf{u} \otimes \mathbf{u} + \frac{1}{2}gh^2\mathbf{I} \\ hc\mathbf{u} \end{matrix} \right\}. \quad (20)$$

Assuming that the sediment transport is always in the flow direction, the numerical flux \mathbf{q}_b^* is defined as in [51]:

$$\mathbf{q}_b^* = \begin{cases} \mathbf{q}_b^+ & \text{if } \hat{\mathbf{u}} \cdot \mathbf{n} \geq 0 \\ \mathbf{q}_b^- & \text{if } \hat{\mathbf{u}} \cdot \mathbf{n} < 0 \end{cases}, \quad (21)$$

where $\hat{\mathbf{u}}$ is the Roe-averaged velocity defined as

$$\hat{\mathbf{u}} = \frac{\mathbf{u}^+ \sqrt{h^+} + \mathbf{u}^- \sqrt{h^-}}{\sqrt{h^+} + \sqrt{h^-}}. \quad (22)$$

Here and for the rest of this article, superscript $+$ denotes a variable value at ∂K when approaching from the interior of an element K , and $-$ when approaching from the exterior. An upwinding scheme is employed for the numerical bed load flux \mathbf{q}_b^* since computing the eigenvalues of the normal Jacobian matrix for the flux matrix $\mathbf{F}(\mathbf{q})$ requires computationally intensive numerical approximation techniques and does not guarantee real values except in the case where the Grass

model is used for \mathbf{q}_b [47, 48]. Therefore, using numerical flux definitions that involve the eigenvalues of the normal Jacobian matrix for the full system may prove to be unfeasible.

The normal Jacobian matrix $\mathbf{A} = \partial_{\mathbf{r}}(\mathbf{G}\mathbf{n})$ of the remaining part of the system has four real eigenvalues: $\lambda_{1,2} = \mathbf{u} \cdot \mathbf{n} \pm \sqrt{gh}$, $\lambda_{3,4} = \mathbf{u} \cdot \mathbf{n}$. A Godunov-type Harten–Lax–van Leer scheme is used to define the numerical flux for the remaining system [52]:

$$\mathbf{G}_h^* = \begin{cases} \mathbf{G}_h^+ \mathbf{n} & \text{if } S^+ > 0 \\ \mathbf{G}_h^{\text{HLL}} & \text{if } S^+ \leq 0 \leq S^- \\ \mathbf{G}_h^- \mathbf{n} & \text{if } S^- < 0 \end{cases}, \quad (23)$$

where $\mathbf{G}_h = \mathbf{G}(\mathbf{r}_h)$, the truncated characteristic speeds S^+ and S^- are

$$S^+ = \min(\mathbf{u}^+ \cdot \mathbf{n} - \sqrt{gh^+}, \mathbf{u}^- \cdot \mathbf{n} - \sqrt{gh^-}), \quad (24a)$$

$$S^- = \max(\mathbf{u}^+ \cdot \mathbf{n} + \sqrt{gh^+}, \mathbf{u}^- \cdot \mathbf{n} + \sqrt{gh^-}), \quad (24b)$$

and the Harten–Lax–van Leer flux $\mathbf{G}_h^{\text{HLL}}$ is

$$\mathbf{G}_h^{\text{HLL}} = \frac{1}{S^- - S^+} ((S^- \mathbf{G}_h^+ - S^+ \mathbf{G}_h^-) \mathbf{n} - S^+ S^- (\mathbf{r}_h^+ - \mathbf{r}_h^-)). \quad (25)$$

A hybridized discontinuous Galerkin scheme may be used to define the numerical flux through $\hat{\mathbf{r}}_h \in \mathbf{M}_h^{p,d+2}$, an approximation to \mathbf{r} over the mesh skeleton called the numerical trace [53]:

$$\mathbf{G}_h^* = \hat{\mathbf{G}}_h \mathbf{n} + \boldsymbol{\tau}(\mathbf{r}_h - \hat{\mathbf{r}}_h), \quad (26)$$

where $\hat{\mathbf{G}}_h = \mathbf{G}(\hat{\mathbf{r}}_h)$, and $\boldsymbol{\tau} = \lambda_{\max}(\hat{\mathbf{r}}_h)$ is the stabilization parameter defined as the maximum eigenvalue of the normal Jacobian matrix \mathbf{A} :

$$\lambda_{\max}(\mathbf{r}) = |\mathbf{u} \cdot \mathbf{n}| + \sqrt{gh}. \quad (27)$$

The numerical trace $\hat{\mathbf{r}}_h \in \mathbf{M}_h^{p,d+2}$ must be such that the numerical flux is conserved across all internal edges in the mesh skeleton, and boundary conditions are satisfied at all boundary edges through the boundary operator \mathbf{B}_h defined according to an imposed boundary condition [53]:

$$\langle \mathbf{G}_h^*, \boldsymbol{\mu} \rangle_{\partial \mathcal{T}_h \setminus \partial \Omega_h} + \langle \mathbf{B}_h, \boldsymbol{\mu} \rangle_{\partial \mathcal{T}_h \cap \partial \Omega_h} = 0 \quad \forall \boldsymbol{\mu} \in \mathbf{M}_h^{p,d+2}. \quad (28)$$

Eq.(18) and Eq.(28) along with the definition of \mathbf{q}_b^* form a system of equations that is used to solve for an approximate solution $\mathbf{q}_h \in \mathbf{V}_h^{p,d+3}$. The boundary condition operator \mathbf{B}_h is defined as

$$\mathbf{B}_h = \mathbf{A}^+ \mathbf{r}_h - |\mathbf{A}| \hat{\mathbf{r}}_h - \mathbf{A}^- \mathbf{r}_\infty, \quad (29)$$

where $\mathbf{A}^\pm = \frac{1}{2}(\mathbf{A} \pm |\mathbf{A}|)$, and \mathbf{r}_∞ is the weakly imposed boundary state [53]. For a slip wall boundary condition, \mathbf{B}_h is defined as

$$\mathbf{B}_h = \hat{\mathbf{r}}_h - \mathbf{r}_{\text{slip}}, \quad (30)$$

where $\mathbf{r}_{\text{slip}} = \{(h)_h \quad (h\mathbf{u})_h - ((h\mathbf{u})_h \cdot \mathbf{n})\mathbf{n} \quad (hc)_h\}^T$ is a state with its normal velocity component truncated [53].

In order to generate \mathcal{S}_2 , a numerical solution operator for the dispersive correction part of the presented hydro-sediment-morphodynamic model, Eq.(6) is written as a system of first order equations using the definition for operator \mathcal{T} [44]:

$$\begin{cases} \nabla \cdot (h^{-1}\mathbf{w}_1) - h^{-3}w_2 = 0 \\ \mathbf{w}_1 - \frac{1}{3}\nabla w_2 - \frac{1}{2}h^{-1}w_2\nabla b + \frac{1}{2}\nabla(h\nabla b \cdot \mathbf{w}_1) + \mathbf{w}_1\nabla b \otimes \nabla b = \mathbf{s}(\mathbf{q}) \end{cases}, \quad (31)$$

where $\mathbf{s}(\mathbf{q}) = \alpha^{-1}gh\nabla\zeta + h\mathcal{Q}_1(\mathbf{u})$. A discontinuous Galerkin finite element discretization for Eq.(31) forms a global system of equations. A hybridized discontinuous Galerkin formulation can be used to reduce the dimension of the global system of equations. Therefore, the hybridized discontinuous Galerkin method developed by Samii and Dawson in [44] is employed to treat numerically Eq.(31) to obtain an approximate solution $\mathbf{w}_{1h} \in \mathbf{V}_h^{p,d}$. The result is then used in the dispersive correction to seek an approximate solution $\mathbf{q}_h \in \mathbf{V}_h^{p,d+3}$ that satisfies the variational formulation

$$(\partial_t \mathbf{q}_h, \mathbf{v})_{\mathcal{T}_h} + (\mathbf{D}_h, \mathbf{v})_{\mathcal{T}_h} = 0 \quad \forall \mathbf{v} \in \mathbf{V}_h^{p,d+3}, \quad (32)$$

where $\mathbf{D}_h = \mathbf{D}(\mathbf{q}_h)$. High order derivatives of \mathbf{u}_h , present in $\mathcal{Q}_1(\mathbf{u}_h)$, are computed weakly using a discontinuous Galerkin method with centered numerical fluxes.

In the developed depth-averaged hydro-sediment-morphodynamic model, it is assumed that the water depth h is bounded from below by a positive value. This assumption implemented by a wetting-drying algorithm which ensures that the water depth remains positive. The numerical solution operator \mathcal{S}_2 does not affect the water depth; therefore, the wetting-drying algorithm should work in conjunction with the numerical solution operator for the SHSM equations \mathcal{S}_1 . In the presented work, the wetting-drying algorithm developed for the nonlinear shallow water equations by Bunya *et al.* in [54] is adapted to the SHSM equations. In the adapted version of the Bunya *et al.* wetting-drying algorithm, the sediment term hc in the SHSM equations is treated the same way as the momentum term $h\mathbf{u}$ and the rest of the algorithm remains the same. The bed update part of the equations does not affect the water depth and, therefore, it does not require the wetting-drying algorithm. Finally, in the dispersive correction part of the equations the wet-dry front is modeled as a slip wall boundary.

Using the Green-Naghdi equations as the hydrodynamic part of the presented model allows capturing wave dispersion effects; however, the Green-Naghdi equations are limited to parts of the problem domain that are free from discontinuities in numerical solutions [43]. This poses certain limitations on the application of the Green-Naghdi equations, e.g. wave breaking phenomena in surf zones present themselves as a water depth discontinuity in numerical solutions. While the Green-Naghdi equations cannot accurately resolve wave

breaking, the nonlinear shallow water equations are more suitable for such areas [43]. Using the Strang operator splitting allows switching to the nonlinear shallow water equations from the Green-Naghdi equations by setting $\mathcal{S}_2 = 1$ in regions with discontinuities in numerical solutions. Thus, a discontinuity detection criterion is required to dynamically switch to $\mathcal{S}_2 = 1$. In the presented work, the numerical solution algorithm is augmented with the water depth discontinuity detection criterion adopted by Duran and Marche in [43] from Krivodonova *et al.* [55]. A water depth discontinuity is identified over an element K if the parameter [55, 43]

$$\mathbb{I}_K = \frac{\sum_{F \in \partial K_{\text{in}}} |\int_F (h^+ - h^-) dX|}{\mathfrak{h}_K^{\frac{p+1}{2}} |\partial K_{\text{in}}| \|h\|_{L^\infty(K)}} \quad (33)$$

is greater than a specified threshold that is typically $O(1)$. In this description of the parameter \mathbb{I}_K , \mathfrak{h}_K is the element diameter, ∂K_{in} are the inflow faces of the element where $\mathbf{u} \cdot \mathbf{n} < 0$, and $|\partial K_{\text{in}}|$ is the total length of the inflow faces.

Since \mathcal{S}_2 is not applied in regions with discontinuities in the numerical solutions, a slope limiting is not needed for the dispersive correction part of the presented model. However, whenever discontinuities occur in the numerical solutions to the SHSM equations a slope limiting algorithm is required in order to remove the oscillations at sharp discontinuities and to preserve numerical stability. Thus, the Cockburn-Shu limiter [56] is incorporated into the numerical solution algorithm and applied in conjunction with the operator \mathcal{S}_1 . The details of the limiter are not presented here, but readers are encouraged to consult the original source.

4. Numerical experiments and discussion

The developed numerical model has been implemented in a software framework written in C++ programming language with the use of open source scientific computing libraries, such as Eigen [57], Blaze [58], and PETSc [59]. The software has been parallelized for shared and distributed memory systems with the use of a hybrid OpenMP+MPI programming, and HPX [60]. Performance comparison between the hybrid programming and HPX has been performed by Bremer *et al.* in [36].

The presented numerical model is validated in five numerical examples. In the first four set-up only the numerical solution operator for the SHSM equations is validated against four dam break experiments. In these experiments the dispersive wave effects are negligible; therefore, $\mathcal{S}_2 = 1$ in the simulations. The last example uses the full dispersive wave hydro-sediment-morphodynamic model to simulate water waves, sediment transport, and bed morphodynamics caused by solitary wave runs over a sloping beach.

The first-order Dubiner polynomials from [61] are used for the approximating space \mathbf{V}_h , and the first-order Legendre polynomials are used for the approximating space \mathbf{M}_h . In all presented examples, numerical solutions are computed

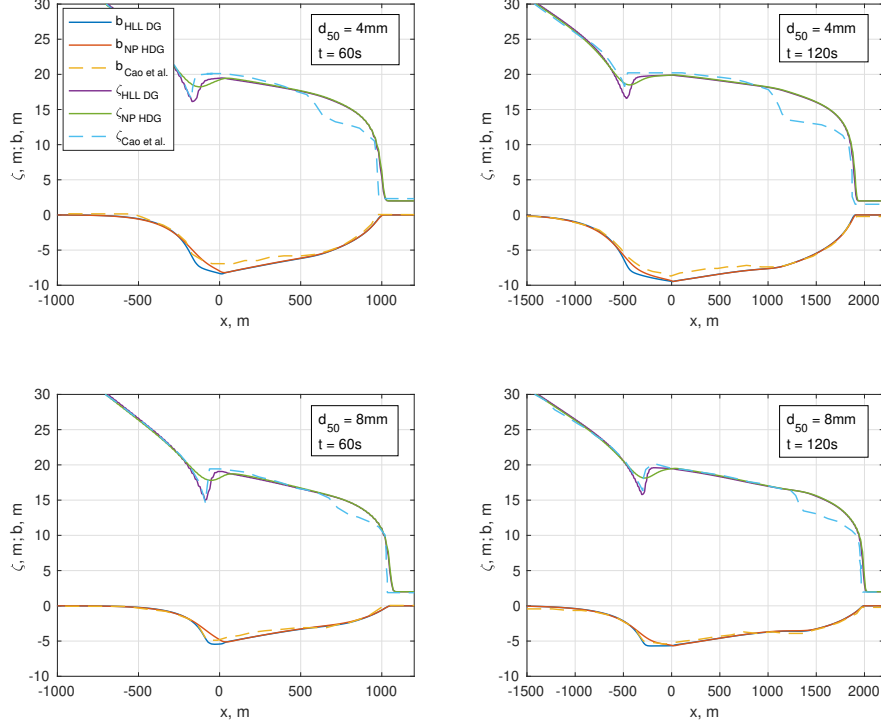


Figure 2: Free surface elevation and bathymetry from the 1D dam break simulation compared with Cao *et al.* experiment [17].

using two different definitions of the numerical flux \mathbf{G}_h^* : (1) the Harten–Lax–van Leer discontinuous Galerkin scheme (HLL DG), (2) the Nguyen-Peraire hybridized discontinuous Galerkin scheme (NP HDG). Consequently, the numerical results obtained using these two definitions for the numerical flux are compared against each other.

4.1. 1D dam break

In this numerical experiment the SHSM equations are used to simulate a 1D dam break over a mobile bed. Initial conditions for this experiment are set as a clear ($c_0(x) = 0$) still water ($\mathbf{u}_0(x) = 0$) with its depth distributed as

$$h_0(x) = \begin{cases} 40 & \text{if } x \leq 0 \\ 2 & \text{if } x > 0 \end{cases}, \quad (34)$$

and the bathymetry set to $b_0(x) = 0$. The mobile bed in this experiment has the sediment density $\rho_s = 2650 \text{ kg/m}^3$, the bed porosity $p = 0.4$, the critical Shields parameter $\theta_c = 0.045$, and the mean sediment particle size d_{50} set as 4mm

and 8mm for two separate simulation runs. For the sediment entrainment rate model, the calibration parameter is set as $\phi = 0.015$. The bed load transport is not considered in this numerical experiment by setting $\mathbf{q}_b = 0$. The bottom friction force is introduced into the model through the source term $\mathbf{S}(\mathbf{q})$ by setting

$$\mathbf{f} = \frac{gn^2}{h^{1/3}}|\mathbf{u}|\mathbf{u}, \quad (35)$$

with the Manning's roughness coefficient $n = 0.03$.

The problem domain $\Omega = (-5000, 5000) \times (-10, 10) \text{ m}^2$ is partitioned into a finite element mesh with 500×1 square cells each containing 2 triangular elements. The explicit Euler time stepping scheme is employed with the time step $\Delta t = 0.1\text{s}$. Two simulations with varying mean sediment particle sizes are run for 2 minutes, and their results are compared to the numerical experiments carried out for the same 1D dam break problem by Cao *et al.* in [17]. The results of the numerical simulations at $t = \{60, 120\}\text{s}$ for $d_{50} = \{4, 8\}\text{mm}$ are presented in Fig.2. Smaller sediment particle sizes imply larger magnitude for sediment entrainment rate E , which presents itself as a larger bed erosion for $d_{50} = 4\text{mm}$. The numerical results for both the free surface elevation, ζ , and the bathymetry, b , are in good agreement with the results obtained by Cao *et al.* The numerical results obtained with HLL DG and NP HDG schemes closely match each other except in the area of the hydraulic jump where NP HDG scheme provides a smoother solution for the free surface elevation.

4.2. 1D dam break with wetting-drying

This example simulates a 1D dam break over a mobile dry bed and is used to validate the wetting-drying algorithm employed in the presented numerical model. Numerical simulations for this experiment are performed with the SHSM equations where water is initially in clear still state, the water depth is set to

$$h_0(x) = \begin{cases} 0.1 & \text{if } x \leq 0 \\ 0 & \text{if } x > 0 \end{cases}, \quad (36)$$

and the initial bathymetry is $b_0(x) = 0$. Two physical experiments have been performed for this setup: (1) the Louvain experiment by Fraccarollo and Capart [62], (2) the Taipei experiment by Capart and Young [63]. These experiments are set up similarly except for the sediment properties. In the Louvain experiment the sediment density $\rho_s = 1540 \text{ kg/m}^3$, the bed porosity $p = 0.3$, the critical Shields parameter $\theta_c = 0.05$, and the mean sediment particle size $d_{50} = 3.5\text{mm}$. On the other hand, in the Taipei experiment the sediment density $\rho_s = 1048 \text{ kg/m}^3$, the bed porosity $p = 0.28$, the critical Shields parameter $\theta_c = 0.05$, and the mean sediment particle size $d_{50} = 6.1\text{mm}$. The calibration parameter for the sediment entrainment rate model, ϕ , is set as 4.0 for the Louvain experiment, and 2.5 for the Taipei experiment. In both experiments, the bed load transport is disregarded by setting $\mathbf{q}_b = 0$, and the Manning's friction model from Eq.(35) is used for the bottom friction force with $n = 0.025$.

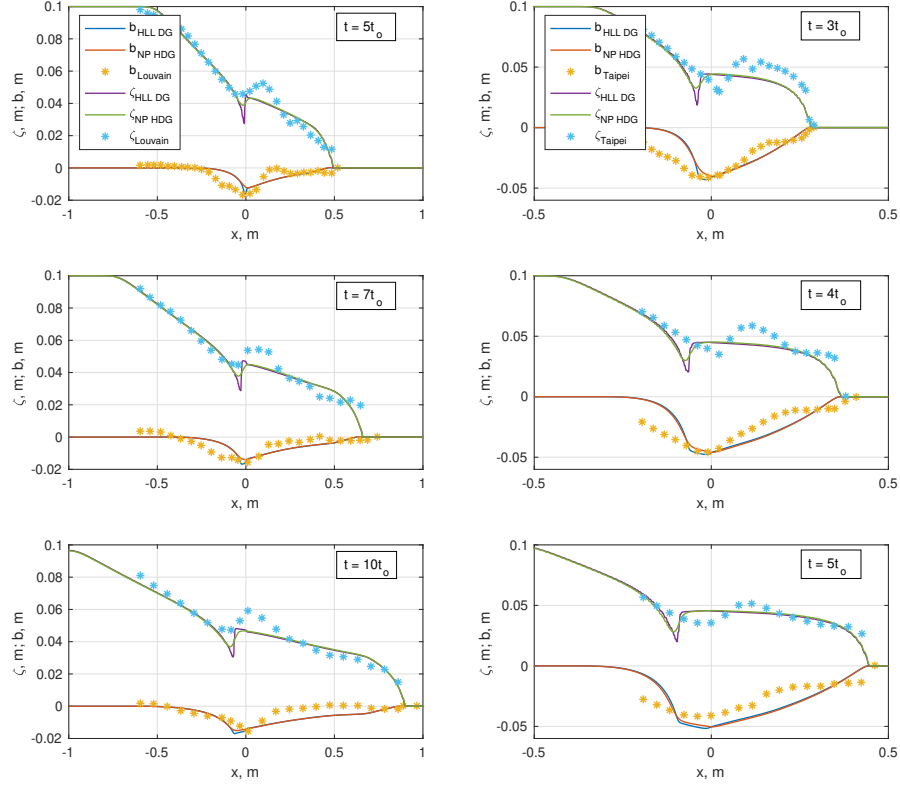


Figure 3: Free surface elevation and bathymetry from the 1D dam break with wetting-drying simulations compared with the Louvain [62] and Taipei [63] experiments.

The problem domain $\Omega = (-1, 1) \times (-2 \cdot 10^{-3}, 2 \cdot 10^{-3}) \text{ m}^2$ is partitioned into a finite element mesh with 500×1 square cells each containing two triangular elements. The explicit Euler time stepping scheme with the time step $\Delta t = 5 \cdot 10^{-4} \text{ s}$ is used to propagate simulations in time for 1s. The simulations of the 1D dam break over mobile dry bed are carried out with the parameters from the Louvain and Taipei experiments. The results are compared with the Louvain experiment at $t = \{5t_0, 7t_0, 10t_0\}$ and with the Taipei experiment at $t = \{3t_0, 4t_0, 5t_0\}$, where $t_0 = \sqrt{g/h_0} \approx 0.101 \text{ s}$ ($h_0 = 0.1 \text{ m}$), in Fig.3. The numerical solution algorithm successfully models the wetting-drying process while providing sufficiently accurate numerical results for the free surface elevation, ζ , and the bathymetry, b . Similar to the previous example, HLL DG and NP HDG results closely match each other everywhere other than the hydraulic jump area.

4.3. 2D flume with abrupt widening

A 2D dam break is simulated in an "L-shaped" flume which is 0.25m wide in its initial 4m and has an abrupt widening on one side to 0.5m for the remaining

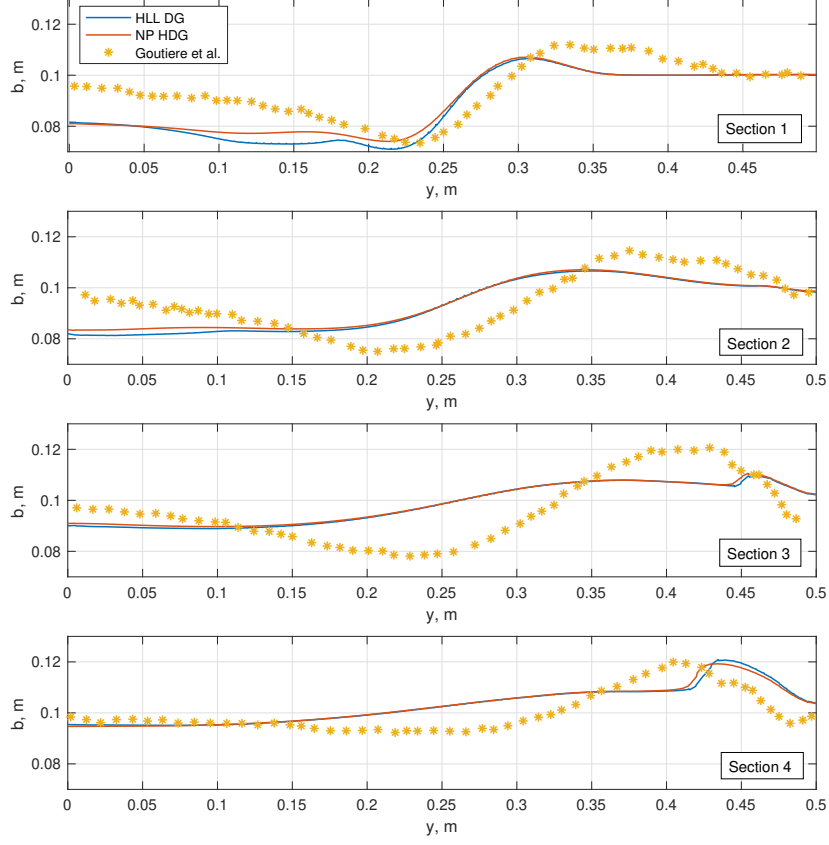


Figure 4: Sediment erosion/deposition measurements from the 2D flume with abrupt widening experiment compared with Goutiere *et al.* results [64].

2m. The flume bed is covered with 0.1m of sediment ($b_0(x) = 0.1$) with the following properties: the sediment density $\rho_s = 2630 \text{ kg/m}^3$, the bed porosity $p = 0.39$, the critical Shields parameter $\theta_c = 0.047$, the mean sediment particle size $d_{50} = 1.72 \text{ mm}$. In this experiment, only the suspended load is taken into account while setting the calibration parameter for the sediment entrainment rate model, ϕ , to 0.35. Initial conditions for the SHSM equations simulations are clear still water with its initial depth

$$h_0(x) = \begin{cases} 0.25 & \text{if } x \leq 3 \\ 0 & \text{if } x > 3 \end{cases}, \quad (37)$$

which implies that the abrupt expansion of the flume is located 1m downstream from the dam break location. The Manning's friction model from Eq.(35) is

used for the bottom friction force with $n = 0.0165$.

The "L-shaped" problem domain Ω for this simulation is partitioned into nearly $4 \cdot 10^4$ triangular elements. The explicit Euler time integration scheme is used for this numerical simulation with the time step $\Delta t = 2 \cdot 10^{-4}$ s. The simulation is run for 20s after which the sediment erosion/deposition measurements are taken at 4 lateral sections located at $x = \{4.1(\text{S1}), 4.2(\text{S2}), 4.3(\text{S3}), 4.4(\text{S4})\}$ m. These measurements are compared with the results of the physical experiment performed by Goutiere *et al.* in [64] in Fig.4. The results of the numerical simulation generally agree with the results of the physical experiment. A general tendency for sediment erosion on the left side and sediment deposition on the right side of the flume is captured in the numerical simulation. The model is also able to capture large sediment deposition on the right side at Sections 3 and 4 where the water flow experiences sudden deceleration due to an impact with the side wall [64]. No significant differences can be observed between HLL DG and NP HDG schemes in this example.

4.4. 2D partial dam break

A partial 2D dam break is simulated in a flume that consist of two 3.6m wide reservoirs that are connected by a 1m long and 1m wide channel with a gate in the middle, which is removed at the beginning of the experiment to simulate a partial dam break. The channel connects the reservoirs along their longitudinal axes. The wet reservoir that holds water is 10m long, and the dry reservoir is 15m long. The bed of the dry reservoir is covered by 0.085m of sediment with the sediment density $\rho_s = 2630 \text{ kg/m}^3$, the bed porosity $p = 0.42$, the critical Shields parameter $\theta_c = 0.047$, and the mean sediment particle size $d_{50} = 1.61 \text{ mm}$. The bed load transport is not taken into account in this experiment, and the calibration parameter for the sediment entrainment rate model $\phi = 0.05$. Initially, the wet reservoir water is in clear still state and is 0.47m deep. The bottom friction force is modeled with the Manning's friction model from Eq.(35) with $n = 0.0165$.

The problem domain Ω for this numerical experiment is partitioned into over 10^5 triangular elements. The numerical simulation is propagated in time with the explicit Euler time stepping scheme with the time step $\Delta t = 5 \cdot 10^{-4}$ s. After 20s of the numerical simulation, the sediment erosion/deposition measurements are taken at 3 longitudinal sections of the dry reservoir located at $y = \{0.2(\text{S1}), 0.7(\text{S2}), 1.45(\text{S3})\}$ m away from the longitudinal axis of the reservoir. Fig.5 presents the measurements and compares them with the results of the physical experiment performed by Soares-Frazão *et al.* in [65]. The results of the numerical simulation are in good agreement with the results of the physical experiment. The sediment is mostly eroded near the channel, where the bed is nearly completely scoured away and deposited downstream by the water flow from the dam break, as is evident from the measurements at Section 1. In this example, HLL DG and NP HDG schemes did not lead to significantly different numerical solutions.

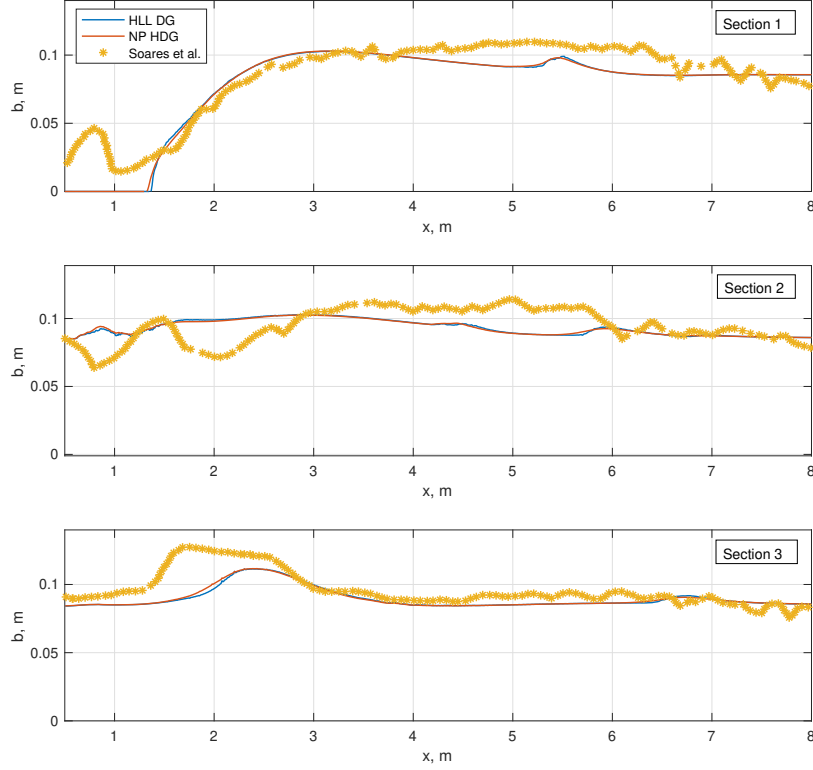


Figure 5: Sediment erosion/deposition measurements from the 2D partial dam break experiment compared with Soares-Frazão *et al.* results [65].

4.5. Solitary wave over a sloping beach

In this experiment, the full dispersive wave hydro-sediment-morphodynamic model is used to simulate water waves, and subsequent sediment transport and bed evolution during run up and run down of a solitary wave over a linearly sloping beach. This experiment showcases a number of features of the presented model: (1) the use of the Green-Naghdi equations as a hydrodynamic component of the model since wave dispersion effects play a significant role during run up of a solitary wave over a sloping beach, (2) switching to the nonlinear shallow water equations as a hydrodynamic model in swash zones since solitary waves in this experiment have a sufficiently high amplitude to experience wave breaking, (3) solitary waves that run over a sloping beach in this experiment cause significant erosion/deposition of the beach bed; thus, the ability of the model to estimate sediment transport and bed morphology can be evaluated. Initial conditions for solitary waves in this experiment are characterized by equations

$$h_0(x) = H_0 + a_0 \operatorname{sech}^2(\kappa(x - x_0)), \quad (h\mathbf{u})_0(x) = c_0 h_0(x) - c_0 H_0, \quad (38)$$

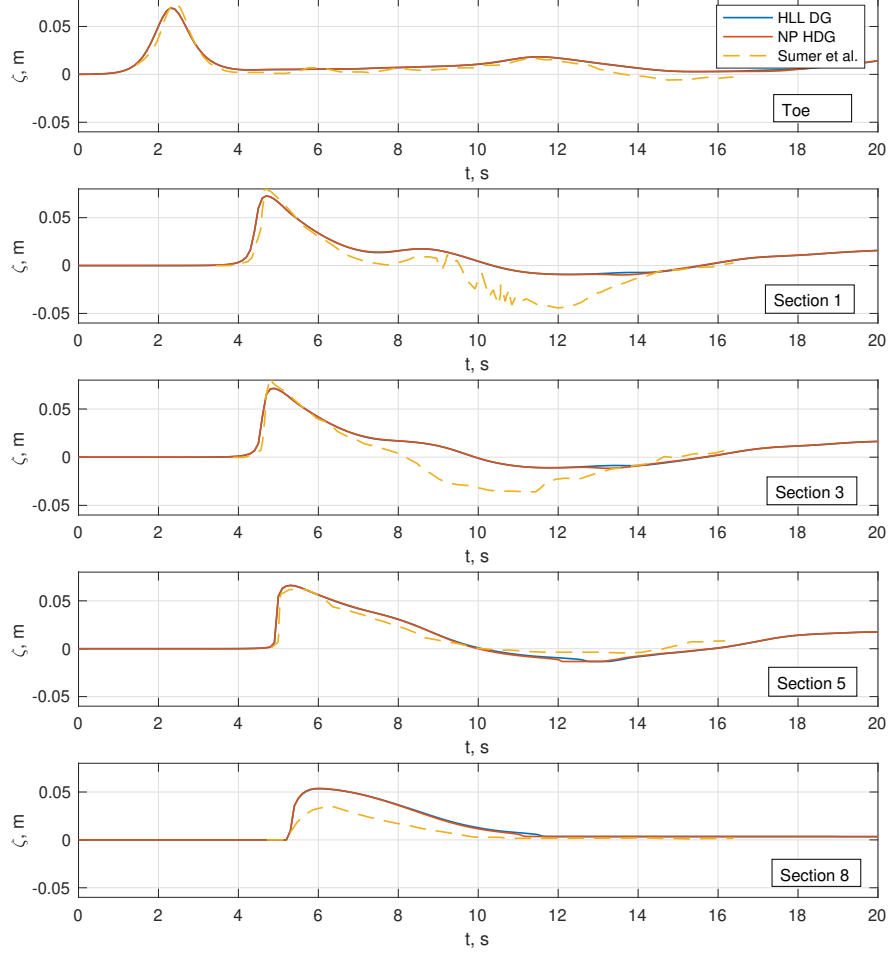


Figure 6: Free surface elevation measurements at 5 measuring stations compared to the experimental results by Sumer *et al.* [66].

where a_0 is the solitary wave height, x_0 the initial wave position, and

$$\kappa = \frac{\sqrt{3a_0}}{2H_0\sqrt{H_0 + a_0}}, \quad c_0 = \sqrt{g(H_0 + a_0)}. \quad (39)$$

Initially, a simulation has been performed over a rigid bed to validate the dispersive wave hydrodynamic model. To carry out this numerical simulation, the problem domain $\Omega = (-10, 10) \times (-2.5 \cdot 10^{-2}, 2.5 \cdot 10^{-2}) \text{ m}^2$ is partitioned into a finite element mesh comprised of 400×1 square cells containing two triangular elements. A two-stage second-order Runge-Kutta method is used to perform time integration with the time step $\Delta t = 5 \cdot 10^{-3} \text{ s}$. The Manning's

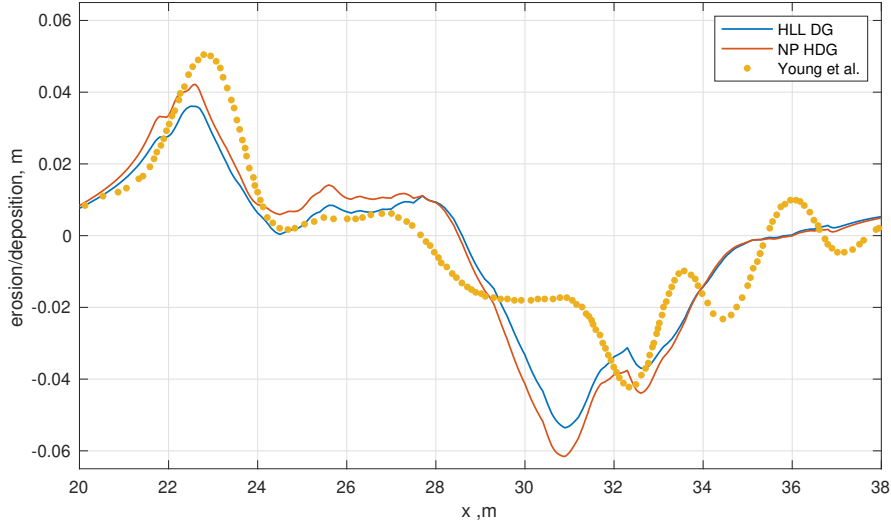


Figure 7: Sediment erosion/deposition measurements for a simulation with the suspended load transport compared with the results by Young *et al.* [67].

roughness coefficient $n = 0.03$ is used for the bottom friction force. The toe of the sloping beach for this simulation is located at $x = 0$ where an initially flat bed starts climbing linearly up at a 1:14 rate. The parameters for the solitary wave in this simulation are: $H_0 = 0.4\text{m}$, $a_0 = 0.071\text{m}$, and $x_0 = -5\text{m}$. This simulation setup corresponds to the solitary wave run over a sloping beach experiment performed by Sumer *et al.* [66]. Fig.6 presents numerical solutions for the free surface elevations recorded at 5 measuring stations located at $x = \{0.0(\text{Toe}), 4.63(\text{S1}), 4.87(\text{S3}), 5.35(\text{S5}), 5.85(\text{S8})\}\text{m}$ during 20s of the simulation and compares them to the experimental results provided by Sumer *et al.* The experimental results suggest that wave breaking occurs somewhere between Sections 3 and 5. This is accurately captured with the dispersive wave hydrodynamic model. However, the free surface elevation measurements at the onshore Section 8 show that the hydrodynamic model is less precise in resolving water waves in the swash zone. Subsequently, the hydrodynamic model is unable to simulate accurately the water motion during the run down stage. Nevertheless, considering complexities associated with modeling water motion induced by solitary waves over a sloping beach, the results of the simulation can be regarded as satisfactory.

To validate the sediment transport and bed morphodynamic part of the model, solitary wave run simulations have been performed over the problem domain $\Omega = (-8, 42) \times (-5 \cdot 10^{-2}, 5 \cdot 10^{-2})\text{m}^2$. The problem domain is partitioned into 500×1 square cells each containing two triangular elements, and a two stage second-order Runge-Kutta method with the time step $\Delta t = 2.5 \cdot 10^{-3}\text{s}$ is

used for temporal discretization. The toe of the sloping beach in the simulation is located at $x = 12\text{m}$ where the flat rigid bed starts climbing at 1:15 rate. The sloping part of the beach is covered with mobile sediment with the sediment density $\rho_s = 2650\text{ kg/m}^3$, the bed porosity $p = 0.4$, the critical Shields parameter $\theta_c = 0.045$, the mean sediment particle size $d_{50} = 0.2\text{mm}$. The Manning's roughness coefficient $n = 0.008$ is used for the bottom friction force. The solitary wave in this simulation is parametrized with $H_0 = 1\text{m}$, $a_0 = 0.6\text{m}$, and $x_0 = 2\text{m}$. A physical experiment with the same setup has been performed by Young *et al.* in [67] where a number of solitary waves have been run over a sloping beach and subsequent sediment erosion/deposition has been recorded. Two simulations are performed: (1) a simulation where only the suspended load transport is taken into account with its results presented in Fig.7, and (2) a simulation where both the suspended and bed load transport are considered with its results presented in Fig.8. For the suspended load, the calibration parameter for the sediment entrainment rate model, ϕ , is set to 0.35; and the Grass model with $A = 2 \cdot 10^{-4}$ is used as a model for the bed load flux \mathbf{q}_b . In both of these simulations sediment erosion/deposition measurements are taken after 3 solitary waves have been run over the sloping beach for 2m each, which is a sufficient time for water to substantially settle. The results of these measurements are compared with the experimental results by Young *et al.* and they are in good agreement. The experimental results indicate that [67]: (1) during the initial run up sediment is entrained in water and deposited onshore at the maximum excursion point where the water flow stalls, (2) during the run down process a shallow high velocity flow causes net sediment erosion in the region between $x = 24\text{m}$ and $x = 35\text{m}$, (3) this entrained sediment is then deposited offshore in the vicinity of the hydraulic jump, which is formed by the retreating water, due to sudden deceleration of the sediment-rich flow. The numerical model is able to capture the sediment transport and bed morphodynamics features observed in the experiment accurately.

5. Conclusions

A dispersive wave hydro-sediment-morphodynamic model has been developed by introducing the dispersive term of a single parameter variation of the Green-Naghdi equations into the SHSM equations. The model can be used to simulate water waves, and the resulting sediment transport and bed morphodynamic processes in areas where wave dispersion effects are prevalent. A numerical solution operator has been developed for the model which employs the second-order Strang operator splitting technique. In order to employ this technique, the dispersive term has been singled out for a separate numerical treatment with a hybridized discontinuous Galerkin method developed by Samii and Dawson in [44], and Harten–Lax–van Leer discontinuous Galerkin, and Nguyen-Peraire hybridized discontinuous Galerkin schemes have been developed for the remaining SHSM equations. The splitting technique makes it possible to select regions where the dispersive term is not applied, e.g. in wave breaking regions where the dispersive wave model is no longer valid. The numerical model is

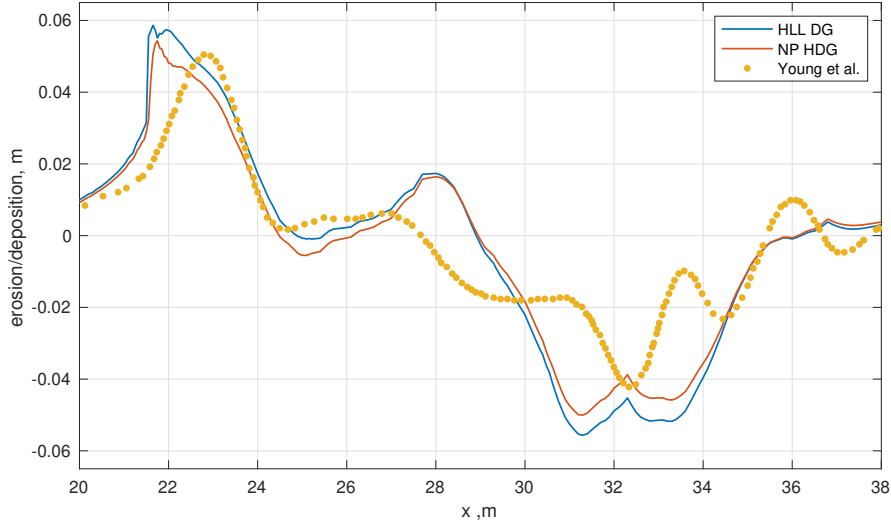


Figure 8: Sediment erosion/deposition measurements for a simulation with the suspended and bed load transport compared with the results by Young *et al.* [67].

augmented with a wave breaking detection mechanism that can dynamically determine regions where the dispersive term is not applied. To facilitate the use of the developed model in problems where water may completely recede from parts of the problem domain, the wetting-drying algorithm by Bunya *et al.* [54] has been incorporated into the numerical model.

The numerical model has been validated against a number of numerical examples. Dam break simulations have been performed to validate the numerical solution schemes developed for the SHSM equations. The results of the simulations indicate that the developed schemes are able to capture hydro-sediment-morphodynamic processes with a sufficient accuracy. Since empirical models are used for the suspended and bed load transport, a close calibration for the empirical models' parameters may be required to improve the accuracy of the presented model. Simulations of a solitary wave run-up over a sloping beach have been performed to validate the full dispersive wave hydro-sediment-morphodynamic model. The results of the simulations indicate that the use of the presented model is justified for flows where the wave dispersion effects are prevalent. Subsequently, the use of the presented model for such flows accurately captures sediment transport and bed morphodynamic processes driven by these flows.

6. Acknowledgments

This work has been supported by funding from the National Science Foundation Grant 1854986, and the Portuguese government through Fundação para

a Ciência e a Tecnologia (FCT), I.P., under the project DGCOAST (UTAP-EXPL/MAT/0017/2017). Authors would like to acknowledge the support of the Texas Advanced Computing Center through the allocation TG-DMS080016N used in the parallel computations of this work.

References

- [1] E. Meyer-Peter, R. Müller, Formulas for bed-load transport, Proceedings of 2nd meeting of the International Association for Hydraulic Structures Research (1948) 39–64.
- [2] R. Fernandez Luque, R. van Beek, Erosion And Transport Of Bed-Load Sediment, *Journal of Hydraulic Research* 14 (2) (1976) 127–144. doi:10.1080/00221687609499677.
- [3] P. Nielsen, Coastal Bottom Boundary Layers and Sediment Transport, Advanced series on ocean engineering, World Scientific, 1992.
- [4] J. S. Ribberink, Bed-load transport for steady flows and unsteady oscillatory flows, *Coastal Engineering* 34 (1) (1998) 59 – 82. doi:10.1016/S0378-3839(98)00013-1.
- [5] L. O. Amoudry, A Review on Coastal Sediment Transport Modelling, <http://nora.nerc.ac.uk/id/eprint/8360> (2008).
- [6] L. O. Amoudry, A. J. Souza, Deterministic Coastal Morphological and Sediment Transport Modeling: a Review and Discussion, *Reviews of Geophysics* 49 (2). doi:10.1029/2010RG000341.
- [7] W. Wu, W. Rodi, T. Wenka, 3D Numerical Modeling of Flow and Sediment Transport in Open Channels, *Journal of Hydraulic Engineering* 126 (1) (2000) 4–15. doi:10.1061/(ASCE)0733-9429(2000)126:1(4).
- [8] H.-W. Fang, G.-Q. Wang, Three-Dimensional Mathematical Model of Suspended-Sediment Transport, *Journal of Hydraulic Engineering* 126 (8) (2000) 578–592. doi:10.1061/(ASCE)0733-9429(2000)126:8(578).
- [9] R. Marsooli, W. Wu, Three-Dimensional Numerical Modeling of Dam-Break Flows with Sediment Transport over Movable Beds, *Journal of Hydraulic Engineering* 141 (1) (2015) 04014066. doi:10.1061/(ASCE)HY.1943-7900.0000947.
- [10] W. Wu, *Computational River Dynamics*, CRC Press, London, 2007. doi:10.4324/9780203938485.
- [11] Z. Cao, C. Xia, G. Pender, Q. Liu, Shallow Water Hydro-Sediment-Morphodynamic Equations for Fluvial Processes, *Journal of Hydraulic Engineering* 143 (5) (2017) 02517001. doi:10.1061/(ASCE)HY.1943-7900.0001281.

- [12] H. Xiao, Y. L. Young, J. H. Prévost, Hydro- and morpho-dynamic modeling of breaking solitary waves over a fine sand beach. Part II: Numerical simulation, *Marine Geology* 269 (3) (2010) 119 – 131. doi:10.1016/j.margeo.2009.12.008.
- [13] F. Zhu, N. Dodd, The morphodynamics of a swash event on an erodible beach, *Journal of Fluid Mechanics* 762 (2015) 110–140. doi:10.1017/jfm.2014.610.
- [14] D.-H. Kim, H2D morphodynamic model considering wave, current and sediment interaction, *Coastal Engineering* 95 (2015) 20 – 34. doi:10.1016/j.coastaleng.2014.09.006.
- [15] G. Incelli, N. Dodd, C. E. Blenkinsopp, F. Zhu, R. Briganti, Morphodynamical modelling of field-scale swash events, *Coastal Engineering* 115 (2016) 42 – 57. doi:10.1016/j.coastaleng.2015.09.006.
- [16] R. Briganti, A. Torres-Freyermuth, T. E. Baldock, M. Brocchini, N. Dodd, T.-J. Hsu, Z. Jiang, Y. Kim, J. C. Pintado-Patiño, M. Postacchini, Advances in numerical modelling of swash zone dynamics, *Coastal Engineering* 115 (2016) 26 – 41. doi:10.1016/j.coastaleng.2016.05.001.
- [17] Z. Cao, G. Pender, S. Wallis, P. Prof, Computational dam-break hydraulics over erodible sediment bed, *Journal of Hydraulic Engineering* 130 (7) (2004) 689–703. doi:10.1061/(ASCE)0733-9429(2004)130:7(689).
- [18] J. Zhao, I. Özgen Xian, R. Hinkelmann, F. Simons, D. Liang, Comparison of capacity and non-capacity sediment transport models for dam break flow over movable bed, CRC Press, London, 2016, pp. 522–527. doi:10.1201/9781315623207-96.
- [19] J. Zhao, I. Özgen Xian, D. Liang, T. Wang, R. Hinkelmann, A depth-averaged non-cohesive sediment transport model with improved discretization of flux and source terms, *Journal of Hydrology* 570 (2019) 647 – 665. doi:10.1016/j.jhydrol.2018.12.059.
- [20] P. Hu, Y. Lei, J. Han, Z. Cao, H. Liu, Z. He, Computationally efficient modeling of hydro-sediment-morphodynamic processes using a hybrid local time step/global maximum time step, *Advances in Water Resources* 127 (2019) 26 – 38. doi:10.1016/j.advwatres.2019.03.006.
- [21] S. Li, C. J. Duffy, Fully coupled approach to modeling shallow water flow, sediment transport, and bed evolution in rivers, *Water Resources Research* 47 (3). doi:10.1029/2010WR009751.
- [22] F. Benkhaldoun, I. Elmahi, S. Sari, M. Seaid, An unstructured finite-volume method for coupled models of suspended sediment and bed load transport in shallow-water flows, *International Journal for Numerical Methods in Fluids* 72 (9) (2013) 967–993. doi:10.1002/flid.3771.

- [23] X. Liu, J. A. I. Sedano, A. Mohammadian, A robust coupled 2-D model for rapidly varying flows over erodible bed using central-upwind method with wetting and drying, *Canadian Journal of Civil Engineering* 42 (8) (2015) 530–543. doi:10.1139/cjce-2014-0524.
- [24] X. Liu, A. Mohammadian, A. Kurganov, J. A. Infante Sedano, Well-balanced central-upwind scheme for a fully coupled shallow water system modeling flows over erodible bed, *Journal of Computational Physics* 300 (2015) 202 – 218. doi:10.1016/j.jcp.2015.07.043.
- [25] X. Liu, A. Beljadid, A coupled numerical model for water flow, sediment transport and bed erosion, *Computers & Fluids* 154 (2017) 273 – 284. doi:10.1016/j.compfluid.2017.06.013.
- [26] C. Xia, Z. Cao, G. Pender, A. Borthwick, Numerical algorithms for solving shallow water hydro-sediment-morphodynamic equations, *Engineering Computations* 34 (2017) 00–00. doi:10.1108/EC-01-2016-0026.
- [27] G. Kesserwani, A. Shamkhalchian, M. J. Zadeh, Fully Coupled Discontinuous Galerkin Modeling of Dam-Break Flows over Movable Bed with Sediment Transport, *Journal of Hydraulic Engineering* 140 (4) (2014) 06014006. doi:10.1061/(ASCE)HY.1943-7900.0000860.
- [28] M. Clare, J. Percival, A. Angeloudis, C. Cotter, M. Piggott, Hydro-morphodynamics 2D modelling using a discontinuous Galerkin discretisation (Jan 2020). doi:10.31223/osf.io/tpqvy.
- [29] D. H. Zhao, H. W. Shen, G. Q. Tabios, J. S. Lai, W. Y. Tan, Finite-Volume Two-Dimensional Unsteady-Flow Model for River Basins, *Journal of Hydraulic Engineering* 120 (7) (1994) 863–883. doi:10.1061/(ASCE)0733-9429(1994)120:7(863).
- [30] K. Anastasiou, C. T. Chan, Solution of the 2D shallow water equations using the finite volume method on unstructured triangular meshes, *International Journal for Numerical Methods in Fluids* 24 (11) (1997) 1225–1245. doi:10.1002/(SICI)1097-0363(19970615)24:11<1225::AID-FLD540>3.0.CO;2-D.
- [31] P. Sleight, P. Gaskell, M. Berzins, N. Wright, An unstructured finite-volume algorithm for predicting flow in rivers and estuaries, *Computers & Fluids* 27 (4) (1998) 479 – 508. doi:10.1016/S0045-7930(97)00071-6.
- [32] V. Aizinger, C. Dawson, A discontinuous Galerkin method for two-dimensional flow and transport in shallow water, *Advances in Water Resources* 25 (1) (2002) 67 – 84. doi:10.1016/S0309-1708(01)00019-7.
- [33] T. H. Yoon, S.-K. Kang, Finite Volume Model for Two-Dimensional Shallow Water Flows on Unstructured Grids, *Journal of Hydraulic Engineering* 130 (7) (2004) 678–688. doi:10.1061/(ASCE)0733-9429(2004)130:7(678).

- [34] E. J. Kubatko, J. J. Westerink, C. Dawson, *hp* Discontinuous Galerkin methods for advection dominated problems in shallow water flow, *Computer Methods in Applied Mechanics and Engineering* 196 (1) (2006) 437 – 451. doi:10.1016/j.cma.2006.05.002.
- [35] A. Samii, K. Kazhyken, C. Michoski, C. Dawson, A Comparison of the Explicit and Implicit Hybridizable Discontinuous Galerkin Methods for Non-linear Shallow Water Equations, *Journal of Scientific Computing* 80 (3) (2019) 1936–1956. doi:10.1007/s10915-019-01007-z.
- [36] M. Bremer, K. Kazhyken, H. Kaiser, C. Michoski, C. Dawson, Performance Comparison of HPX Versus Traditional Parallelization Strategies for the Discontinuous Galerkin Method, *Journal of Scientific Computing* 80 (2) (2019) 878–902. doi:10.1007/s10915-019-00960-z.
- [37] A. E. Green, P. M. Naghdi, A derivation of equations for wave propagation in water of variable depth, *Journal of Fluid Mechanics* 78 (2) (1976) 237–246. doi:10.1017/S0022112076002425.
- [38] F. Chazel, D. Lannes, F. Marche, Numerical Simulation of Strongly Nonlinear and Dispersive Waves Using a Green-Naghdi Model, *Journal of Scientific Computing* 48 (1) (2011) 105–116. doi:10.1007/s10915-010-9395-9.
- [39] P. Bonneton, F. Chazel, D. Lannes, F. Marche, M. Tissier, A splitting approach for the fully nonlinear and weakly dispersive Green-Naghdi model, *Journal of Computational Physics* 230 (4) (2011) 1479 – 1498. doi:10.1016/j.jcp.2010.11.015.
- [40] N. Panda, C. Dawson, Y. Zhang, A. B. Kennedy, J. J. Westerink, A. S. Donahue, Discontinuous Galerkin methods for solving Boussinesq-Green-Naghdi equations in resolving non-linear and dispersive surface water waves, *Journal of Computational Physics* 273 (2014) 572 – 588. doi:10.1016/j.jcp.2014.05.035.
- [41] D. Lannes, F. Marche, A new class of fully nonlinear and weakly dispersive Green-Naghdi models for efficient 2D simulations, *Journal of Computational Physics* 282 (2015) 238 – 268. doi:10.1016/j.jcp.2014.11.016.
- [42] A. Duran, F. Marche, Discontinuous-Galerkin Discretization of a New Class of Green-Naghdi Equations, *Communications in Computational Physics* 17 (3) (2015) 721–760. doi:10.4208/cicp.150414.101014a.
- [43] A. Duran, F. Marche, A discontinuous Galerkin method for a new class of Green-Naghdi equations on simplicial unstructured meshes, *Applied Mathematical Modelling* 45 (2017) 840 – 864. doi:10.1016/j.apm.2017.01.030.
- [44] A. Samii, C. Dawson, An explicit hybridized discontinuous Galerkin method for Serre-Green-Naghdi wave model, *Computer Methods*

- in *Applied Mechanics and Engineering* 330 (2018) 447 – 470. doi:10.1016/j.cma.2017.11.001.
- [45] F. Marche, Combined Hybridizable Discontinuous Galerkin (HDG) and Runge-Kutta Discontinuous Galerkin (RK-DG) formulations for Green-Naghdi equations on unstructured meshes, *Journal of Computational Physics* 418 (2020) 109637. doi:10.1016/j.jcp.2020.109637.
 - [46] S. Li, C. J. Duffy, Fully coupled approach to modeling shallow water flow, sediment transport, and bed evolution in rivers, *Water Resources Research* 47 (3). doi:10.1029/2010WR009751.
 - [47] M. J. Castro Díaz, E. D. Fernández-Nieto, A. M. Ferreiro, Sediment transport models in Shallow Water equations and numerical approach by high order finite volume methods, *Computers & Fluids* 37 (3) (2008) 299 – 316. doi:10.1016/j.compfluid.2007.07.017.
 - [48] S. Cordier, M. Le, T. Morales de Luna, Bedload transport in shallow water models: Why splitting (may) fail, how hyperbolicity (can) help, *Advances in Water Resources* 34 (8) (2011) 980 – 989. doi:10.1016/j.advwatres.2011.05.002.
 - [49] A. J. Grass, *Sediment Transport by Waves and Currents*, SERC London Centre for Marine Technology, Report No. FL29.
 - [50] G. Strang, On the Construction and Comparison of Difference Schemes, *SIAM Journal on Numerical Analysis* 5 (3) (1968) 506–517. doi:10.1137/0705041.
 - [51] C. Mirabito, C. Dawson, E. J. Kubatko, J. J. Westerink, S. Bunya, Implementation of a discontinuous Galerkin morphological model on two-dimensional unstructured meshes, *Computer Methods in Applied Mechanics and Engineering* 200 (1) (2011) 189 – 207. doi:10.1016/j.cma.2010.08.004.
 - [52] A. Harten, P. D. Lax, B. v. Leer, On Upstream Differencing and Godunov-Type Schemes for Hyperbolic Conservation Laws, *SIAM Review* 25 (1) (1983) 35–61. doi:10.1137/1025002.
 - [53] N. Nguyen, J. Peraire, Hybridizable discontinuous Galerkin methods for partial differential equations in continuum mechanics, *Journal of Computational Physics* 231 (18) (2012) 5955 – 5988. doi:10.1016/j.jcp.2012.02.033.
 - [54] S. Bunya, E. J. Kubatko, J. J. Westerink, C. Dawson, A wetting and drying treatment for the Runge–Kutta discontinuous Galerkin solution to the shallow water equations, *Computer Methods in Applied Mechanics and Engineering* 198 (17) (2009) 1548 – 1562. doi:10.1016/j.cma.2009.01.008.

- [55] L. Krivodonova, J. Xin, J.-F. Remacle, N. Chevaugeon, J. Flaherty, Shock detection and limiting with discontinuous Galerkin methods for hyperbolic conservation laws, *Applied Numerical Mathematics* 48 (3) (2004) 323 – 338. doi:10.1016/j.apnum.2003.11.002.
- [56] B. Cockburn, C. Shu, Runge-Kutta discontinuous Galerkin methods for convection-dominated problems, *Journal of Scientific Computing* 16 (3) (2001) 173–261. doi:10.1023/A:1012873910884.
- [57] G. Guennebaud, B. Jacob, et al., Eigen v3, www.eigen.tuxfamily.org (2010).
- [58] K. Iglberger, Blaze C++ Linear Algebra Library, www.bitbucket.org/blaze-lib (2012).
- [59] S. Balay, S. Abhyankar, M. F. Adams, J. Brown, P. Brune, K. Buschelman, L. Dalcin, A. Dener, V. Eijkhout, W. D. Gropp, D. Karpeyev, D. Kaushik, M. G. Knepley, D. A. May, L. C. McInnes, R. T. Mills, T. Munson, K. Rupp, P. Sanan, B. F. Smith, S. Zampini, H. Zhang, H. Zhang, Portable, Extensible Toolkit for Scientific Computation, www.mcs.anl.gov/petsc (2019).
- [60] H. Kaiser, B. A. Leebach, T. Heller, M. Simberg, A. Bergé, J. Biddiscombe, A. Bikineev, G. Mercer, A. Schäfer, K. Huck, A. S. Lemoine, T. Kwon, J. Habraken, M. Anderson, M. Copik, S. R. Brandt, M. Stumpf, D. Bourgeois, D. Blank, S. Jakobovits, V. Amatya, L. Viklund, Z. Khatami, P. Diehl, T. Pathak, D. Bacharwar, S. Yang, E. Schnetter, STELLAR-GROUP/hpx: HPX V1.4.1: The C++ Standards Library for Parallelism and Concurrency (Feb. 2020). doi:10.5281/zenodo.3675272.
- [61] M. Dubiner, Spectral methods on triangles and other domains, *Journal of Scientific Computing* 6 (4) (1991) 345–390. doi:10.1007/BF01060030.
- [62] L. Fraccarollo, H. Capart, Riemann wave description of erosional dam-break flows, *Journal of Fluid Mechanics* 461 (2002) 183–228. doi:10.1017/S0022112002008455.
- [63] H. Capart, D. L. Young, Formation of a jump by the dam-break wave over a granular bed, *Journal of Fluid Mechanics* 372 (1998) 165–187. doi:10.1017/S0022112098002250.
- [64] L. Goutiere, S. Soares-Frazão, Y. Zech, Dam-break flow on mobile bed in abruptly widening channel: experimental data, *Journal of Hydraulic Research* 49 (3) (2011) 367–371. doi:10.1080/00221686.2010.548969.
- [65] S. Soares-Frazão, R. Canelas, Z. Cao, L. Cea, H. M. Chaudhry, A. Die Moran, K. El Kadi, R. Ferreira, I. Fraga Cadórniga, N. Gonzalez-Ramirez, M. Greco, W. Huang, J. Imran, J. Le Coz, R. Marsooli, A. Paquier, G. Pender, M. Pontillo, J. Puertas, B. Spinewine, C. Swartenbroekx, R. Tsubaki,

- C. Villaret, W. Wu, Z. Yue, Y. Zech, Dam-break flows over mobile beds: experiments and benchmark tests for numerical models, *Journal of Hydraulic Research* 50 (4) (2012) 364–375. doi:10.1080/00221686.2012.689682.
- [66] B. M. Sumer, M. B. Sen, I. Karagali, B. Ceren, J. Fredsøe, M. Sottile, L. Zilioli, D. R. Fuhrman, Flow and sediment transport induced by a plunging solitary wave, *Journal of Geophysical Research: Oceans* 116 (C1). doi:10.1029/2010JC006435.
- [67] Y. L. Young, H. Xiao, T. Maddux, Hydro- and morpho-dynamic modeling of breaking solitary waves over a fine sand beach. Part I: Experimental study, *Marine Geology* 269 (3) (2010) 107 – 118. doi:10.1016/j.margeo.2009.12.009.